The process of surface carburization and high temperature wear behavior of infiltrated W-Cu composites

Wenge Chen[a*], Pei Feng[a], Longlong Dong [b,*], Meysam Ahangarkani[c], Shuxin Ren[a], Yongqing Fu[d,*]

[a] School of Materials Science and Engineering, Xi'an University of Technology, Shaanxi, Xi'an, 710048, PR China

[b] Advanced Materials Research Central, Northwest Institute for Nonferrous Metal Research, Xi'an 710016, China

[c] Department of Materials, Malek Ashtar University of Technology, Tehran, Iran

[d] Faculty of Engineering and Environment, Northumbria University, Newcastle upon Tyne, NE1 8ST, UK

Abstract

Tungsten-copper (W-Cu) composites are used as high temperature frictional materials under special service conditions for electromagnetic gun rail and precision guide for rolled pieces due to their good ablation resistance and electrical conductivity. However, they have poor wear resistance at elevated temperatures. In this paper, surface carburization method was applied on the W-20wt.%Cu composite to investigate the mechanisms of carburization and its effects on the high temperature friction behavior

* Corresponding authors:
E-mail: wgchen001@263.net (W.G. Chen), donglong1027@163.com, lldong1027@aliyun.com (L.L. Dong), richard.fu@northumbria.ac.uk (Richard Y.Q. Fu)

of composite. Carburization process has been done at a temperature of 1100 ºC for 30 hours. The obtained results showed that carburizing at 1100 °C with a dwelling time of 30 hours resulted into formation of a carburized layer and a dense intermediate sub-layer on the substrate. Also, the surface carburized layer with a thickness of about 70 µm composed of mixed phases of graphite, WC and W_2C. The hardness of carburized layer (~HV454) was significantly higher than that of substrate (HV223). Also, bending and[S1] strength of the carburized W-Cu composites has been significantly improved, although their electrical conductivity and tensile strength was decreased slightly. The carburization mechanism of the W-Cu composites was found to be dominant by carbon atom diffusion through reaction with W atoms and formation of surface liquid copper, which promoted migration and diffusion of tungsten and carbon at high temperatures. Average coefficients of friction and wear rate of carburized W-Cu composites are all lower than these of un-carburized W-Cu composites owing to the presence of surface carburized layer. Also, formation of $CuWO_4$ at high temperatures reduced the friction and wear resistance of the W-Cu composites.

Keywords: W-Cu composites; Carburizing; Microstructure; Friction and Wear

1. Introduction

Tungsten copper (W-Cu) composites is a non-miscible pseudo-alloy which consist of mixed W and Cu phases and is generally produced using a powder metallurgy technology [1-2]. It has numerous good properties, such as good resistance to arc erosion, good machinability, relatively high strength, and good thermal conductivity, thus has been widely used in electronic seals, high-voltage electrical contacts [3],

electromagnetic railway [4], nozzle throat for rocket engine [5] and oval hole guide for the precision rolling mill [6-7]. However, failure of components during service was frequently initiated from the surface of the composites components, especially when there are various types of surface defects [8-9]. Due to the lower melting point and cooling effect of Cu and the high melting point and high strength of W, W-Cu composites generally show a good performance when they are used as guides and guarding materials. However, they often show premature failures due to their insufficient surface hardness [10]. Therefore, Liu et al. [11] have been reported using of different methods to improve the surface properties of the W-Cu composites, which include surface coating, nanoscale surface sputtering, and surface diffusion processes such as carburization or nitriding.

Surface carburization is widely used in many industries because the process is simple and there is no need for expensive equipment and complicated processes. The process has been traditionally used for iron-steel materials, but recently been extended to titanium and titanium alloys, tungsten alloys, zirconium alloys and other non-ferrous metal materials. For example, He et al. [12] reported that carburization of Ti-48Al-2Cr-2Nb alloy could be achieved at 920 °C with a dwelling time of 2 hrs. A uniform and dense carburized layer was generated on the surfaces of TiAl alloys, and their anti-oxidation and mechanical properties were significantly improved. Li et al. [13] reported that hydrogen-free glow-discharge plasma carburizing of titanium could be conducted in a vacuum of 5×10^{-3} Pa and 99.999% Ar atmosphere. Results showed that the depth of carburized layer was more than 100 μm and the Vickers hardness was ~ 612 HV with a friction coefficient of 0.11. Wang et al. [14] investigated carburization of Ti based composites and formation of TiC layer on the α-Ti substrate and reported that the carburization of a high-density tungsten alloy could be achieved at 950 °C for 5 hrs.

The thicknesses of surface W_2C layer were in the range of 170 μm to 200 μm and the hardness values were varied from HV 388 to HV 525. This treatment had effectively improved the surface hardness of armor piercing bullets, whereas the core of the projectile could be easily broken under a high-speed impact, thus improving its self-sharpening performance and enhancing its piercing ability, which was reported by Jung et al. [15].

However, to the best of our knowledge, there is no any report on the study of the carburization behavior and mechanism of W-Cu composites so far, experimentally or theoretically. In the present study, we will focus our work on solid carburization of the W-20wt.% Cu composites and for the first time; identify their behavior against high temperature friction and wear.

2. Experimental

The W-Cu composites used in this work were fabricated by infiltrating the molten copper into a tungsten porous skeleton. Chen et al. [16] described the detailed preparation process. The nominal weight fractions of W and Cu were 80 wt% and 20 wt%, respectively. The basic properties of the composite materials are listed in Table 1.

Table 1 Physical and mechanical properties of W-Cu composite used in the work.

The specimens of the W-Cu composites were firstly machined into the form of a cylinder with a dimension of Φ60 mm × 30 mm. The surfaces of samples were carefully polished using 240-grade abrasive sandpaper. The sample was embedded inside graphite powders with an average particle size of 150~200 mesh, while 10% sodium carbonate was added as a penetration agent. The buried sample in the graphite powders was placed in an atmospheric carburizing furnace under flowing H_2 atmosphere and

heated to the temperatures of 1100±10°C, the carburization temperature was controlled using a high temperature infrared thermometer (Smart, AS892). The heating rate was 10 °C/min and the holding time at soaking temperature was 30 hours. After carburization, the furnace was cooled down to room temperature.

Fig. 1 Schematic of the carburization experiments for W-Cu composites.

The friction test was done on the carburized sample and un-carburized composites. This test was carried out using an HT-100 pin-on-disc high temperature wear tester. The test condition was dry friction at a high temperature of 900 ºC with normal loads of 5 N and 20 N. The sliding speed during wear testing was 300 r/min. The size of testing sample (i.e., pins) was a diameter of 5 mm and a height of 10 ~ 12 mm. A gray cast iron (HT 250 with a hardness of HB 190) with a diameter of 50 mm and a height of 5 mm was chosen as frictional counterpart. And then the wear rate of W-Cu composites is measured using a MicroXAM 3D surface profilometer system to determine the wear volume. The detailed measured process had been reported by author Xu et al. [17].

Microstructures and fracture morphology of the samples before and after carburization were observed using a scanning electron microscope (SEM, JSM-6700). The chemical elements were analyzed using an energy dispersive X-ray spectroscopy (EDS) and electron probe microanalyser (EPMA) analyzer attached with the SEM. Crystalline structures of the carburized samples were analyzed using an X-ray diffractometer (XRD, XRD-7000S, Cu K-alpha radiation), with a scanning rate of 8 °/min, a scanning range of 2θ of 10 ~ 90 ° and a step size of 0.02°. The different layers

of carburized samples were tested using a layer-by-layer delamination method. The carbon and oxygen concentrations at the different positions of the carburization layer were measured using EPMA.

Mechanical properties of samples before and after carburization treatment were characterized with a three-point bending method using a HT-2402 universal test machine. The size of sample was 5.25 mm × 9.97 mm × 24.6 mm. The bending strength was calculated according to the following equation [18]:

$$\sigma_r = \frac{3FL}{2bh^2} \quad (1)$$

where σ_r is bending strength (MPa), F is the maximum load during fracture (N), L is spacing between two lower supporting points (mm), b is specimen width (mm), and h is specimen thickness (mm). The tensile test was carried out at room temperature at a strain rate of 1 mm/min using a WE-100 universal tester. The hardness of the samples was measured using a micro-Vickers hardness tester (TUKON2100), and the applied load was 200 g with a holding time of 10 s. The electrical conductivity of the samples was measured using a metal electrical conductivity tester (D60K).

3. Results and discussion

In order to verify that the surface of the W-Cu composites was covered with carbon-rich layer, cross-section microstructures of the W-Cu composite after carburization at 1100 ^{o}C were observed using SEM (Fig. 2(a)). Cross-section morphology of the W-Cu composite after carburization is composed of three distinct regions, as shown in Fig. 2(a) (i.e., the loose surface layer; a dens intermediate layer on the substrate). The first loose layer is attributed to various reasons during high

temperature process, such as accumulation of graphite powder, formation of voids due to the partial bonding at high temperature, and channel formation created by evaporation of liquid copper on the surface. Carbon concentration distribution of W-Cu composite after carburization at 1100 ^{o}C for holding time 30 h was exhibited in Fig. 2(b), in which the C atom have diffused into the W-Cu matrix. Also, SEM images and elemental mapping analysis results from surface morphology of the W-Cu composites before and after carburization at 1100 ^{o}C are shown in Fig. 3. In Fig. 3(a_1), the gray and black areas are W and Cu phases, respectively. Also, the SEM image of the uncarburized W-Cu composites reveals compact and smooth. And the Cu phases are homogeneously distributed around the W phase, as observed in Figs. 3(a_2) ~ 3(a_4). As illustrated, after carburization (in Fig. 3(b)), the surface of carburized W-Cu composites (especially W particles) exhibits many edges and corners which are quite rough. There are a large number of small W particles around the Cu phases. It can also be found that the volume fraction of the binder phase or porosity (the dark/black area in Fig. 3(b)) increased significantly because the edges and corners of the W particles are dissolved by the binder phase of Cu in the activation of carbon was reported by Huang [18]. It is also possible that W reacts with carbon to form carbide. In order to determine the phase presence and C distribution in the surface of the carburized W-Cu composites, energy dispersive spectroscopy (EDS) analysis was also perform on the entire surface in Fig. 3(b), the results are shown in Fig. 3 (b_1) ~ 3(b_4). We can found that C atom are distributed on the grain boundaries of W or Cu grains, especially most of C atoms are covered around the W particles, the main reason is that C can be easily transported in

the form of hydrocarbons over a distance of several millimeters up to centimeters on the W-matric composites when they are in the condition of H_2 atmosphere [19]. The precious presence and content of carbon inside the carburized W-Cu composites is identified from the EPMA analysis, as shown in inset of Fig. 3(b_5), indicating the reactions between tungsten and carbon are happened. Also, compared Fig. 3(a_2) with 3(b_2), the Cu and W element distribution in W-Cu composites changed a lot after carburization at 1100^{o}C owing to the formation of carbide and the flowing and solidification of liquid Cu. At the same time, evaporation and spillover of copper cause a decrease in copper content of the surface during high temperatures carburization, as shown inset of Fig. 3(a) and 3(b_5), the copper concentration reduced from 18.87wt.% to 13.94wt.% in the surface layer after carburization. The W particles in the intermediate layer become no longer smooth compared to those in the matrix layer after carburization, and there are many edges and corners, accompanying with a large number of small tungsten particles surrounding the Cu phases, which is consistent with the results shown in Fig. 3(b). From the EPMA analysis of carbon distribution shown in inset of Figs. 3(a) and 3(b_5) (i.e. as shown in the inset tables of these figures), the surface carbon content is higher than the sub-surface carbon content. With the increase of distance from the exposure surface, the carbon content reduces, and finally decreases to zero in the substrate. The result verifies that the carbon elements were diffused into the substrate, and the carburized layer was formed with a thickness of about 40~80 microns. [S2]Combined with Fig. 4(b), the obvious diffusion of C between 100 ~ 200 μm can be observed,, which revealed the average carburized layer is about 70 μm.

Fig. 2 (a) SEM morphology from cross section and (b) carbon concentration distribution of W-Cu composite after carburization at 1100 ^{o}C for holding time 30h.

Fig. 3 SEM surface morphologies and EDS results of W-Cu composites (a, a_1, a_2, a_3) before carburization and (b, b_1, b_2, b_3, b_4, b_5) after carburization at 1100^{o}C, respectively.

The composition and microstructures of the W-Cu composite (in Fig. 2) show three different characteristic regions after carburization treatment. This is mainly because the composite was buried inside graphite, and there is a carbon concentration gradient formed into the sample. Increase of the surface carbon content will reduce the liquid phase formation temperature of the composites was reported by Liu et al. [20], which results in an early formation of the liquid phase of composites at the surface. Carbon atoms react with tungsten to form the WC or W_2C, through dissolving and precipitation of newly formed WC particles, and also through the formation of liquid copper phase on the surface. Because carbon and tungsten atoms have a large affinity at high temperatures, the C atoms could migrate inward and then react with W atoms to form the WC or W_2C. Therefore, the surface content of W decreases, and the outward migration of W to the surface leads to the formation of volume vacancy at reaction sites [21]. This will drive the surface liquid copper to migrate inwards to fill up the volume vacancy due to the tungsten's outward migration. Therefore, the outward migration of the W atoms and the inward migration of liquid copper simultaneously occur in the carburizing process of the W-Cu composites.

Fig. 4(a) is a back-scattered electron image of the carburized W-Cu composites, indicating that the W (green dots) and Cu (red dots) phases are homogeneously distributed inside the matrix. Carbon elements (dark dots) are distributed along the

cross-section of the composites, and the EDS elemental line scan is shown in Fig. 4(b). It can be seen that the copper and tungsten are diffused outward, whereas the carbon is diffused from outside into the composites, on the other hand, the curve oscillation for Cu concentration in Fig. 3(b) is attributed to the melting and flowing during the carburization process, which further validates the previous analysis (Fig. 3).

Fig. 4 (a) SEM mapping image and (b) elemental line scan curves of surface carburized W-Cu composite.

Fig. 5 shows the XRD patterns at different cross-section positions of W-Cu composites after carburization. It can be seen that at the center of the tungsten-copper composites, only the W peak (cf JCPDS file No. 04-0806) and Cu (cf JCPDS file No. 04-0836) peak are detected. After carburization, the surface layer shows the phases of WC (cf JCPDS file No. 51-0939), W_2C (cf JCPDS file No. 20-1315) and graphite or C (cf JCPDS file No. 50-0926). According to the W-C phase diagram [22], tungsten carbides generally have three phases of WC, W_2C and WC_{1-x}. In this study, WC_{1-x} was not detected in the surface and sub-surface. This is because the WC_{1-x} is a high-temperature metastable phase [23] which is easily decomposed into W_2C, WC and W phases during the slow cooling process. Therefore, the carbides on the surface of the carburized specimen are WC and W_2C. In addition, the carbon peak can also be detected in the surface layer, which is related to diffused C without reaction with tungsten.

Fig. 5 XRD results of W-Cu composites after carburization at 1100 ^{o}C in different positions of the sample (a) surface layer, (b) sub-layer, and (c) substrate material.

In order to further understand the effects of carburizing, micro-hardness, bending

strength and electrical conductivity were measured on the samples before and after carburization, and the results are summarized in Table 2. The micro-hardness of the surface layer after carburization is approximately twice that of the surface before carburization, mainly due to the formation of hard carbides and carbon diffused layer. On the contrary, the electrical conductivity of the W-Cu composites was decreased from about 34 IACS% to 32.2 IACS% after carburization, due to the formation of WC and W_2C after carburization. The bending strength of W-Cu composites was increased from a value of 890 MPa before carburization to a value of 1104 MPa after carburization. The main reason is that the maximum stress was subjected to the surface of the samples, and the surface strength of the WCu composites was enhanced after carburizing. Also, the tensile properties change of W-Cu composites after carburization for 30 h at the temperature of 1100 ^{o}C are shown in Fig. 6. It can be seen that the engineering stress-strain curves in Fig. 6 shows a similar trend (i.e. first elastic deformation, followed by plastic deformation until final fracture of the samples). However, the carburized W-Cu composites exhibit higher[S3] yield (YS) and ultimate tensile strength (UTS) rather than the uncarburized composite, i.e. the YS and UTS of carburized W-Cu composites are 204 MPa and 359 MPa, respectively, which are about 23.9% and 27.5% lower than the original composites. These decreases in strength are mainly because the carburized layer with the surface loose layer and the copper evaporation on the surface of the W-Cu composites, as well as the information of the WC and W_2C hard and brittle phases. The decreased tensile strength of the carburized WCu composites are attributed to that the tensile stress is basically uniform along the cross-section of the sample, and the

surface carburized layer has a high strength and low plasticity, which contributes little to the tensile stress.

Table 2 Properties of W-Cu composite before and after carburization at 1100 ^{o}C.

Fig. 6 The tensile stress – strain of W-Cu composites before and after carburization for 30h at the temperature of 1100 ^{o}C.

Figs. 7(a) and (a_1) show the SEM fracture images of original W-Cu composites. W particles in composite mainly have demonstrated inter-granular brittle fracture, as observed in Fig. 7(a_1). Also, each of the W fractures generates one large dimple and because of the extensive stretching of this surface it appears quite featureless, because the porosity sites and solid-solid contacts are the weak point of W-Cu compacts. Thus, the failure of composite with high content of W starts by separation of W/W and develops by producing cleaved W grain after strain hardening the Cu phase and then matrix rupture occurs during the tensile process. Also, the fracture morphologies of the surface region and center of the W-Cu composites after carburization at 1100 ^{o}C are exhibited in Figs. 7(b, b_1) and 7(c, c_1), respectively. The dark and bright areas are W and Cu phases, respectively. It can be seen that there are a lot of dimples on the fractured carburizing surfaces (as indicated by the blue arrow). This is attributed to the surface hardening layer with a large stress owing to the different coefficient of linear expansion of matrix (W and Cu phase) and surface layer materials (C and carbides), which results in the generation of micro-pores due to the differences in the material properties. These pores are then grown and connected along the hardening layer and matrix as well as the boundaries of the W grains. However, from Figs. 7(c) and 7(c_1), no obvious cracks are observed in the matrix of the material. The fracture process has the following

sequences: (1) the separation of W-W interface; (2) the separation of W-Cu interface; (3) the ductile fracture of Cu under the action of stress. Therefore, the key fracture mechanism of the carburized components is a combination of brittle fracture of carbonized layer and cleavage fracture of the substrate. This is consistent with what have been reported in the literature for the fracture characteristics of the W-Cu composites prepared at high temperatures and high pressures [24].

Fig. 7 Fracture morphology of the W-Cu composites before and after carburization at 1100°C with a dwell time of 30h: (a, a_1) Un-carburized W-Cu composites, (b, b_1) surface and (c, c_1) matrix of carburized W-Cu composites.

Based on the above results, the carburizing reaction process and schematic of the W-Cu composites is proposed in Fig. 8. The W-Cu composites are firstly surrounded by graphite flakes, as shown in Fig. 8(a). Because the diameter of the carbon atoms is 0.154 nm, and that of the tungsten atoms is 0.274 nm [25], therefore, C atoms easily diffuse into the interstitial octahedral spaces of the W structures at high temperatures [26]. The carbon atoms continue to diffuse into the W structures, and simultaneously tungsten can also diffuse and migrate into the W-Cu composites due to the formed liquid copper at the surface (as explained above). It is well-known that the carburization rates are controlled by two diffusion mechanism include mass transfer coefficients at the W-Cu surface and carbon atom diffusion in the W-Cu material. In the case of diffusion of C into the W-Cu substrate, since activation energy for grain boundary diffusion is always less than the activation energy for lattice diffusion, diffusion rate of C atoms through W-W grain boundaries is always higher (Fig. 8(b)). Subsequently, the C atoms

initiate to diffuse into W grains as schematically illustrated in Fig. 8(c). This leads to the formation of high C concentrations in the near surface region. As the concentration of C exceeds from solubility limit of C in W, the deposition of C in W will result in the formation of tungsten carbides, such as WC and W_2C, especially at grain boundaries as shown in Fig. 8(d). Finally, the near surface region of carburized W-Cu consists of three different parts including loss layer, intermediate layer and remained matrix.

Fig. 8 The schematic diagram of W-Cu composite carburization process

Carburization process occurs along the cross-section of the sample, and is driven by the carbon concentration gradient [27]. It is well known that the carburizing process is strongly influenced by the carburizing temperature and time, and the rate of carburization is controlled by the initial carbon concentration. Based on the well-known solution of the diffusion equation for a semi-infinite body, with a constant concentration of carbon on the surface, as well as the value of diffusion coefficient (Eq. (2)) [29], the diffusion concentrations of carbon (C_x) can be solved using the Gauss error function in the Fick's Second Law, i.e. (Eq. (3)).[28]:

$$D = 8.91\times10^{-7}\exp(-\frac{224\times10^{3}}{8.314T}) \quad (2)$$

The diffusion concentrations of carbon (C_x) can be solved using the Gauss error function in the Fick's Second Law, i.e.,

$$\frac{C_s - C_x}{C_s - C_0} = erf(\frac{x}{2\sqrt{Dt}}) \quad (3)$$

where t is the time of diffusion, i.e. the carburization dwelling time (hr), x the distance from the diffuser to the interface (mm), C_s is the initial carbon concentration, C_0 is

the carbon concentration at a distance from the surface.

Following two equations present the chemical reactions between W particle and carbon.

$$2W+C \rightarrow W_2C \quad (4)$$

$$W_2C+C \rightarrow 2WC \quad (5)$$

According to the W-C phase diagram [29], the above reactions (4) and (5) occur when the carbon content is over 6.0 wt.% and the temperature is larger than 1000°C. In this study, the W-Cu composites have ~80 wt.% of tungsten content (W%=80 wt.%), and the carbon content from the phase diagram at this W concentration of 80% is 4.0 wt.% (i.e., C%=4.0%). The initial carbon concentration C_0 at the surface can be set as 8.0 wt.% (see Fig. 3(b)) when the time is equal to zero. Simultaneously, it is assumed that the carbon concentration at a distance from the surface is zero.

Based on the Fick's 2nd Law and parameters we used, the distributions of carbon concentration were obtained and the results are shown in Fig. 9. The results indicate that the carbon concentration gradient decreases rapidly in the surface layer of the composites, and then tends to become steady when the carburizing temperature and time are increased. Fig. 9 also shows the measured carbon concentrations along the thickness of the cross-section of samples obtained from the EPMA results. Clearly, there is a good agreement with the experimental results and calculated ones.

Fig. 9 Results of carbon concentration distribution of W-Cu composites after carburization at 1100 ^{o}C, obtained from analysis based on Fick's 2nd Law and experimental measurement.

Fig. 10 presents the friction coefficients of the carburized W-Cu composites tested at 900 ^{o}C under different applied loads measured as a function of sliding time. In generally, the friction process curve and can be divided into several points, and take the average value of the friction coefficient of all points can be considered as the average friction coefficient. The average friction coefficient can be obtained from following equation:

$$\overline{\mu} = \frac{1}{S}\sum \mu_i \Delta s_i \tag{6}$$

in which μ_i is the Instantaneous friction coefficient, Δs_i Incremental braking distance (m), S is braking distance (m).

It can be seen that the test had a point contact with a small amount of area contact, and friction coefficient was not a fixed value and varied at the beginning of the friction test. However, the coefficients maintain a stable value with an increasing of the sliding time. At a low contact load, the friction pair initially did not fully contact with samples, thus there was more variance in the friction values. With the increase of load, the fluctuation of the friction coefficient was decreased and the average friction coefficient values were reduced. At a larger load, it was much quicker to change into a stable wear stage. With the increase of real contact area, the pressure on unit area was smaller than that of the initially contacted one, thus plastic deformation and shear friction were all decreased. The average friction coefficient values of the carburized W-Cu composites are 0.53 and 0.46 under two different applied loads (5N and 20N), respectively. To be compared with, as shown in Figs. 10(a) and (c), the average friction coefficient values

of the untreated W-Cu composites are 0.62 and 0.52 under different applied loads (5 N and 20 N), respectively. Also, the wear rate of carburized W-Cu composite is 0.086 mg/h after the high temperature wear under a 5N applied load, which is much lower than that of un-carburized composites (0.122 mg/h). As shown in Fig. 10 curves (b) and (d), the friction coefficient of the carburized layer is relatively smaller under the high temperature. The hardness value of the surface carburized layer is much higher than that of the un-carburized composites (see Table 2). Also it is well-known that the carbon (graphite) has a good self-lubricating effect, thus the friction coefficient can be further reduced during tests.

Fig. 10 Friction coefficient curve of W-Cu composite after carbonization at 1100 ^{o}C under different applied loads measured and sliding time.

In order to further investigate the phase composition changing of the W-Cu composites after high temperature. XRD was performed on the surface of samples which are subjected to high temperature wear test, and results are shown in Fig. 11. It is revealed that the W and Cu phases on the surface of W-Cu composites were oxidized into oxides such as WO_3 and CuO. The oxides could temporarily protect the W-Cu substrate because they possess high melting point and high hardness. Furthermore, a phase of $CuWO_4$ with brown or yellow color could be formed when the W-Cu composites were subjected to a high-temperature process for a long time [30]. Erdemir [30] reported that the oxides with high ionic potentials showed low shear strength and

good lubricity based on the crystal-chemical model. They pointed out that (1) these oxides exhibit large differences in the ionic potential; and (2) they are more stable thus may lead to lower attraction between sliding surfaces. This could result in much less adhesive forces across the sliding contact interfaces, hence producing the lower friction. In this work, the differences of ionic potential (IP) values of tungsten oxide and copper oxide are quite high (i.e., IP_{WO3}=8.8 and IP_{CuO}=5.6). Based on Erdemir's theory [28], the tungsten-copper oxides of $CuWO_4$ possess a low shear strength, therefore, the friction will be reduced accordingly.

Fig. 11 The surface XRD pattern of the carburized W-Cu composites after high temperature wear.

In order to investigate the influence of oxygen content on the wear behavior of composite at high temperature, the percentage of oxygen at different wear depths of W80-Cu20 composites after wear experiment at 900 ^{o}C for 40 min are shown in Fig. 12, along with the SEM images. The morphologies of Cu and W phases are not clearly observed except that many pits and corrosion products are formed on the uneven worn surface. Also, the oxygen content is the highest on the surface of W80Cu20 composites as shown in Fig. 12(a). With the increase of distance from the exposure surface, the oxygen content decreases gradually. Furthermore, the surface pits in Fig. 12(b) are much shallower than those shown in Fig. 12(a), as a result, partial exposed W particles and grinding traces can be observed in Fig. 12(b). In Fig. 12(c), the morphology is the same as those shown in Fig. 12(a), which indicates that the influence of oxygen content

is limited to the distance within 3 mm from the friction surface in wear condition.

Fig. 12 The content of oxygen and SEM images of W-Cu composite wear at 900 ^{o}C.

4. Conclusion

(1) The carburized layer of W-Cu composites is composed of loose surface carbide layer, dense intermediate layer and substrate. Phases of the surface carburized layer include C, WC and W_2C.

(2) The micro-hardness of the surface layer after carburization is approximately twice that of the surface before carburization, mainly due to the formation of hard carbides and carbon diffused layer. The conductivity of the composites was decreased from about 34 IACS% to 32.2 IACS%.

(3) The bending strength of composites was increased from a value of 890 MPa to a value of 1104 MPa after carburization. YS and UTS of carburized W-Cu composites are 204 MPa and 359 MPa, respectively, which are about 23.9 % and 27.5 % lower than the original composites due to the carburized layer with the surface loose layer and the copper evaporation on the surface of the W-Cu composites, as well as the information of the WC and W_2C hard and brittle phases. Formation of oxide of $CuWO_4$ during high temperature wear is beneficial to reduce friction and wear. Average coefficients of friction for W-Cu composites carburized at 900 ^{o}C under the normal loads of 5 N and 20 N are 0.53 and 0.46, respectively.

Acknowledgements

The authors would like to acknowledge the financial support from Xi'an Science Research Project of China (No. 2017080CG/RC043) and Electrical Materials and

Infiltration Key Laboratory of Shaanxi Province (No. 17JS080), and the financial support from Northwest Institute for Nonferrous Metal Research (K1652-1) and UK Newton Mobility Grant (IE161019) through Royal Society and the National Natural Science Foundation of China, as well as Royal academy of Engineering UK-Research Exchange with China and India. Thanks for the experimental support from professor Y.T. HUANG of Fujian University of Technology.[S4]

References

[1] W.G. Chen, Y.G. Kuang, W.P. Zhou, Current research status of W-Cu composites for high temperature in China, Rare. Metal. Mater. Eng. 33 (1) (2004) 11-14.

[2] L.L. Dong, W.G. Chen, N. Deng, C.H. Zheng, Investigation on arc erosion behaviors and mechanism of W70Cu30 electrical contact materials adding graphene, J. Alloy. Compd. 696 (2017) 923-930.

[3] M. Ahangarkani, K.Zangeneh-Madar, S.Borji, Z.Valefi, Microstructural study on ultra-high temperature erosion mechanism of infiltrated W-10wt%Cu composite, Int. J. Refract. Met. H. 67 (2017) 115-124.

[4] S.Semboshi, AkihiroIwase, T.Takasugi, Surface hardening of age-hardenable Cu–Ti alloy by plasma carburization, Surf. Coat. Tech, 283 (15) (2015) 262-267.

[5] J.X. Liu, J.H. Wang, Q. Li, Z.Y. Chen, P.W. Cong, Study and application of high temperature carburizing process for 18CrNiMo7-6 and 20CrNi2Mo steels, Heat. Treat. Met. 38 (10) (2013) 66-69.

[6] L.L. Dong, M. Ahangarkani, W. Zhang, B. Zhang, W.G. Chen, Y.Q. Fu, Y.S. Zhang, Formation of gradient microstructure and mechanical properties of hot-pressed W-20wt.%Cu composites after sliding friction severe deformation, Mater. Charact. 144 (2018) 325-335.

[7] M.O. Cojocaru, D. Dragomir, L. Druga, Effects of Electromagnetic Induction on Growth Kinetics of Case Hardened Layers, Heat. Treat. 30 (5) (2015) 32-36.

[8] K. Lu, J. Lu, Nanostructured surface layer on metallic materials induced by surface mechanical

attrition treatment, Mater. Sci. Eng. A 38 (7) (2004) 375-377.

[9] X. Wei, D.M. Yu, Z.B. Sun, Z.M. Yang, X.P. Song, B.J. Ding, Arc characteristics and microstructure evolution of WCu contacts during the vacuum breakdown, Vacuum. 107 (2014) 83-89.

[10] P. Yang, J. Y. Zhang, The research status and prospect of the rolled steel guide board material, Equip. Manu. Tech. 12 (2011) 106-108.

[11] G.M. Liu, J.Li, Q.X. Zhang, B. Li, The failure mechanism of the guide rail of H62 brass electromagnetic gun, J. School. Ironc. Eng. 27 (5) (2013) 90-94.

[12] Y.H. He, B.Y. Huang, X.H. Qu, Y.X. Liu, Improvement of oxidation resistance of TiAl based alloy at the elevated temperature by carburization, Chin. J. Mater. Res. 10 (6) (1996) 603-607.

[13] Z.X. Li, J.H. Du, H. Zhou, Z. Xu, L. Zhou, Double-Glow plasma surface carbon implantation of Non-Hydrogen on titanium, Rare. Met. Mater. Eng. 33 (11) (2004) 1174-1177.

[14] L. Wang, S.K. Li, X.G. Song, Research on surface carburization of tungsten heavy alloys, Acta. Arma. 28 (6) (2007) 730-732.

[15] S.W. Jung, S. Lee, S.J. Kang, E. Pyokim, J.W. Noh, W.H. Baek, Control of surface carburization and improvement of dynamic fracture behavior in tungsten heavy alloys, Metall. Mater. Trans. 33A (4) (2002) 1213-1219.

[16] W.G. Chen, B.J. Ding, H. Zhang, Nanocrystal W-Cu electrical contact material by mechanical alloying and hot pressed sintering, Chin. J. Nonferr. Met. 12 (6) (2002) 1221-1228.

[17] J.H. Xu, H.B. Ju, L.H. Yu, Effects of Mo content on the microstructure and friction and wear properties of TiMoN films, Acta Metall. Sin. 48(9) (2012) 1132-1138.

[18] D. William, J.R. Callister, Materials Science and Engineering, Hoken: John Wiley & Sons, Inc., 2003.

[18] P.Y. Huang, Powder Metallurgy Principle. Beijing: Metallurgy Industry Press, 1997.

[19] G. Muhlbauer, G. Kremser, Andreas Bock, J. Weidow, W.D. Schubert, Transition of W2C to WC during carburization of tungsten metal powder, Int. J. Refrac. Met. Hard. Mate. 71, (2018) 141-148.

[20] Y.L. Liu , Y. Gao, J.S. Bao, G.B. Huang, J.W. Xiang, Studies on preparation and properties of functionalizing graphene doped molten salt composites, Inorg. Chem. Indus. 48 (7) (2016) 16-20.

[21] W.B. Zhan, H.B. Wang, S.H. Liang, X.M. Liu, X.Y. Song, Acceleration effect of cobalt on carburization of tungsten at low temperature, J. Alloy. Compd. 732 (2018) 429-435.

[22] S.A. Humphry-Baker, W.E. Lee, Oxidation resistant tungsten carbide hardmetals, Scr. Mater. 116 (2016) 67-70.

[23] Q.P. Wei, Z.M. Yu, Z. Chen, X.D. Zhu, P.Z. Liu, Effect of filament radiation length and W-C gradient interlayer on diamond films deposited on high-speed steel, Chin. J. Noferr. Met. 21(11) (2011) 2825-2835.

[24] W.G. Chen, L.L. Dong, H. Zhang, J.L. Song, N. Deng, J.J. Wang, Microstructure characterization of WCu alloy sheets produced by high temperature and high pressure deformation technique, Mat. Lett. 205 (2017) 198-201.

[25] Z.C. Liu, The principle of transformation structure of material, Beijing, Metallurgical Industry Press, 2006.

[26] M. Ahangarkani, K. Zangeneh-Madar, S. Borji, Z. Valefi, Microstructural study on ultra-high temperature erosion mechanism of infiltrated W-10 wt%Cu composite, Int. J. Refrac. Met. Hard. Mate. 67 (2017) 115-124.

[27] S.X. Wang, Y. Liu, Practical heat treatment simulation technology. Beijing: China Machine Industry Press, 2002.

[28] M.G. Liu, A.Q. Chen, The growth behavior of hafnium carbide and its relationship with the diffusion of tungsten at high temperature, Tung. Moly. Mater. 3 (1996) 18-24.

[29] L. Janka, L.M. Berger, J. Norpoth, R. Trache, S. Thiele, C.Tomastik, V. Matikainen, P. Vuoristo, Improving the high temperature abrasion resistance of thermally sprayed Cr3C2-NiCr coatings by WC addition, Surf. Coat. Tech, 337 (15) (2018) 296-305.

[30] Erdemir A. A crystal - chemical approach to lubrication by solid oxides, J. Tribol. Lett. 89 (2) (2000) 97-102.

[30] Erdemir A. A crystal chemical approach to the formulation of self-lubricating nanocomposite coatings, Surf. Coat. Tech. 200 (8) (2005) 1792-1796.

List of Tables captions:

Fig. 1 Schematic of the carburization experiments for W-Cu composites.

Fig. 2 (a) SEM morphology from Cross section and (b) carbon concentration distribution of W-Cu composite after carburization at 1100 ^{o}C for holding time 30h.

Fig. 3 SEM surface morphologies and EDS results of W-Cu composites (a, a_1, a_2, a_3) before carburization and (b, b_1, b_2, b_3, b_4, b_5) after carburization at 1100^{o}C, respectively.

Fig. 4 (a) SEM mapping image and (b) elemental line scan curves of surface carburized W-Cu composite.

Fig. 5 XRD results of W-Cu composites after carburization at 1100^{o}C in different positions of the sample (a) surface layer, (b) sub-layer, and (c) substrate material.

Fig. 6 The tensile stress – strain of W-Cu composites before and after carburization for 30h at the temperature of 1100^{o}C.

Fig. 7 Fracture morphology of the W-Cu composites before and after carburization at 1100^{o}C with a dwell time of 30h: (a, a_1) Uncarburized W-Cu composites, (b, b_1) surface and (c, c_1) matrix of carburized W-Cu composites.

Fig. 8 The schematic diagram of W-Cu composite carburization process

Fig. 9 Results of carbon concentration distribution of W-Cu composites after carburization at 1100^{o}C, obtained from analysis based on Fick's 2nd Law and experimental measurement.

Fig. 10 Friction coefficient curve of W-Cu composite after carbonization at 1100^{o}C under different applied loads measured and sliding time.

Fig. 11 The XRD pattern of the carburized W-Cu composites after high temperature wear.

Fig. 12 The content of oxygen and SEM images of W-Cu composite wear at 900 ^{o}C.

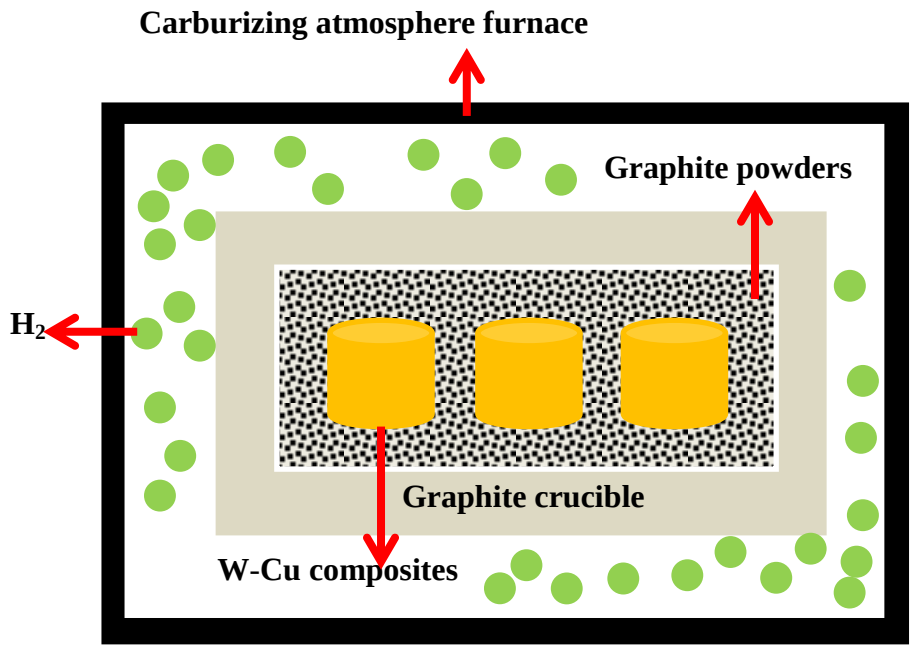

Fig. 1 Schematic of the carburization experiments for W-Cu composites.

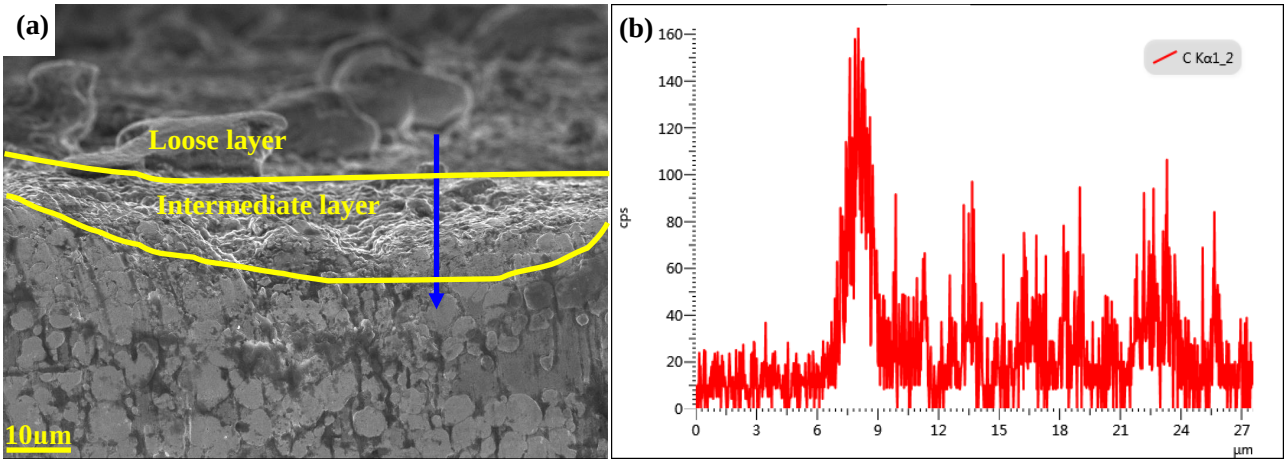

Fig. 2 (a) SEM morphology from Cross section and (b) carbon concentration distribution of W-Cu composite after carburization at 1100 ^{o}C for holding time 30h.

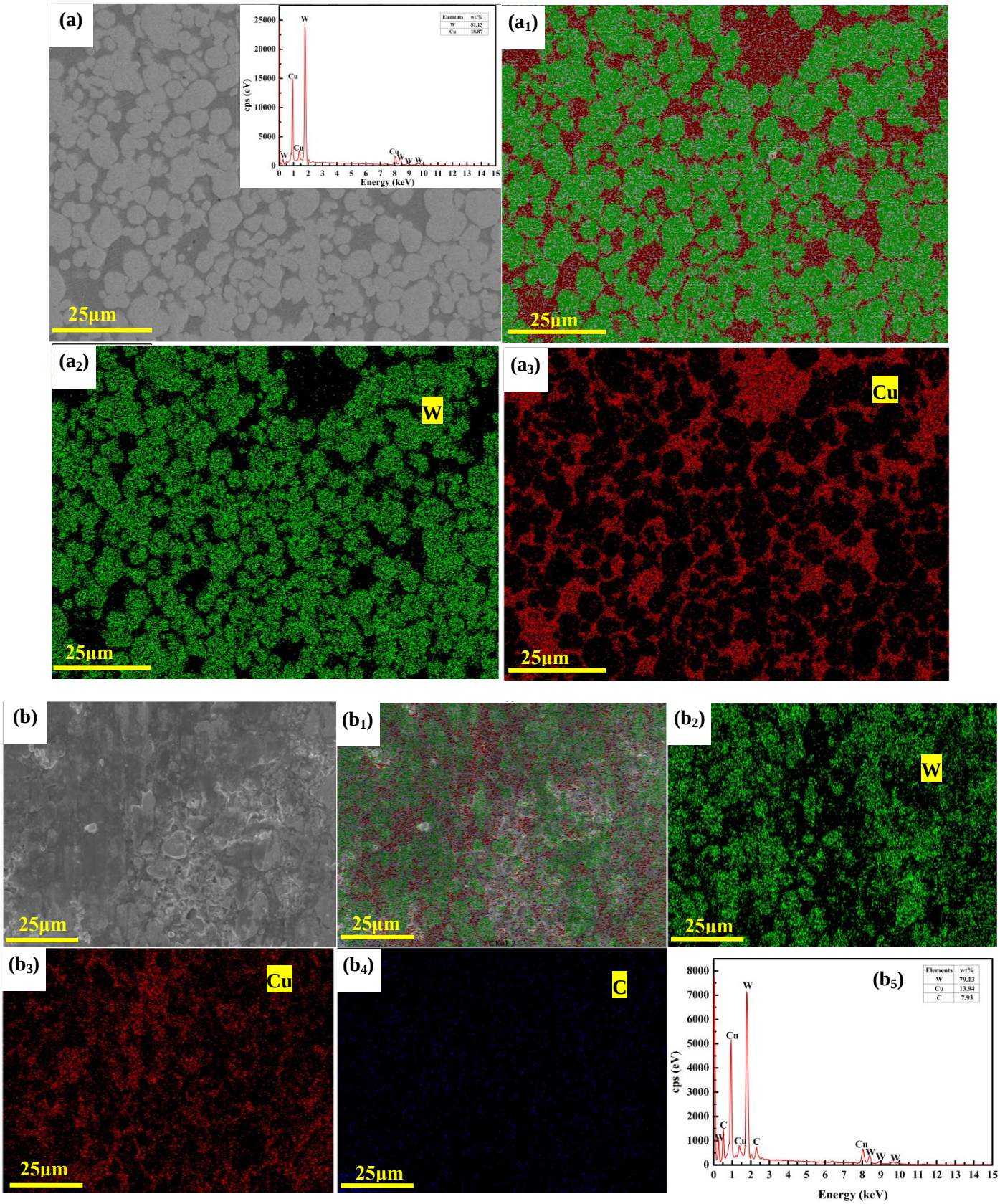

Fig. 3 SEM surface morphologies and EDS results of W-Cu composites (a, a_1, a_2, a_3) before carburization and (b, b_1, b_2, b_3, b_4, b_5) after carburization at 1100°C, respectively.

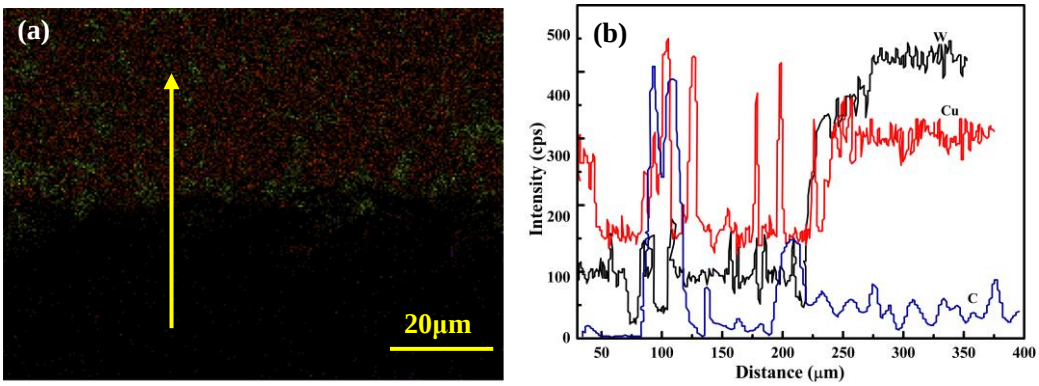

Fig. 4 (a) SEM mapping image and (b) elemental line scan curves of surface carburized W-Cu composite.

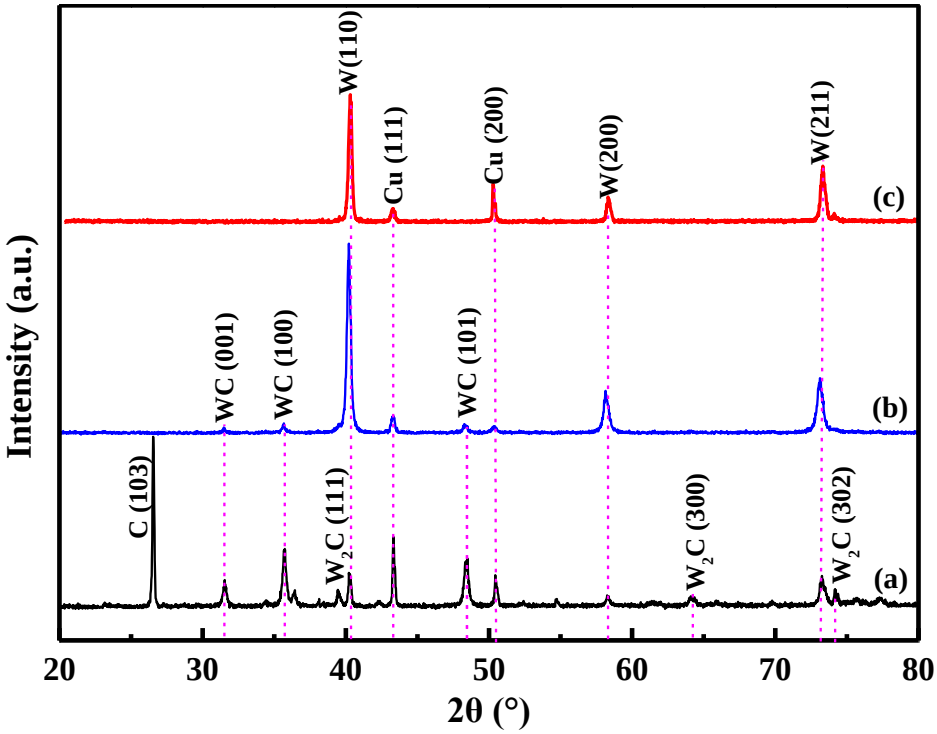

Fig. 5 XRD results of W-Cu composites after carburization at 1100^{o}C in different positions of the sample (a) surface layer, (b) sub-layer, and (c) substrate material.

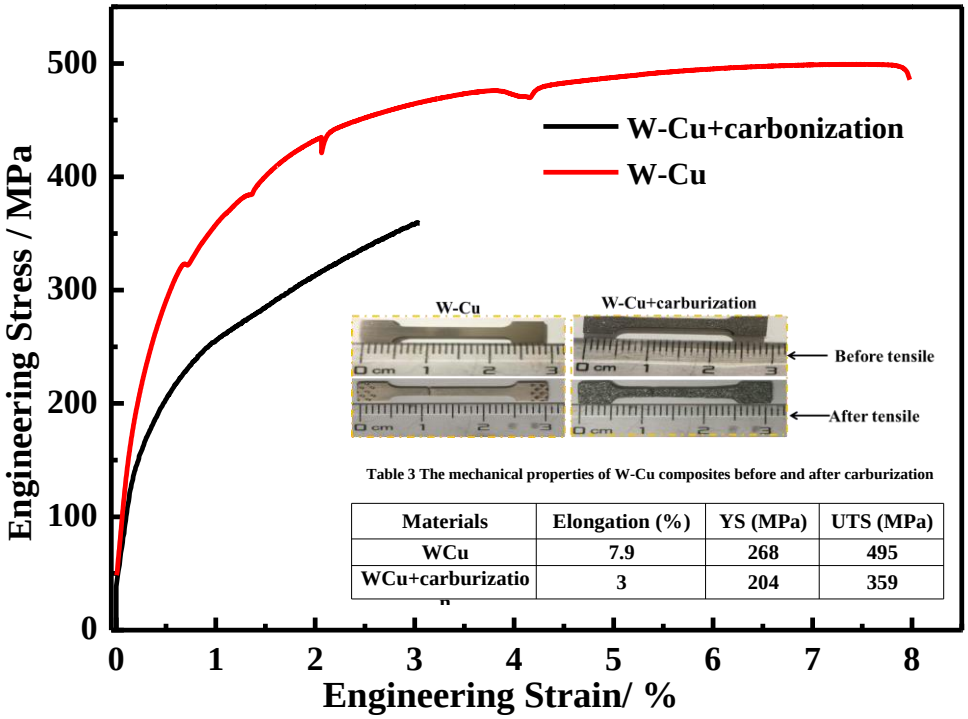

Table 3 The mechanical properties of W-Cu composites before and after carburization

Materials	Elongation (%)	YS (MPa)	UTS (MPa)
WCu	7.9	268	495
WCu+carburizatio n	3	204	359

Fig. 6 The tensile stress – strain of W-Cu composites before and after carburization for 30h at the temperature of 1100^{o}C.

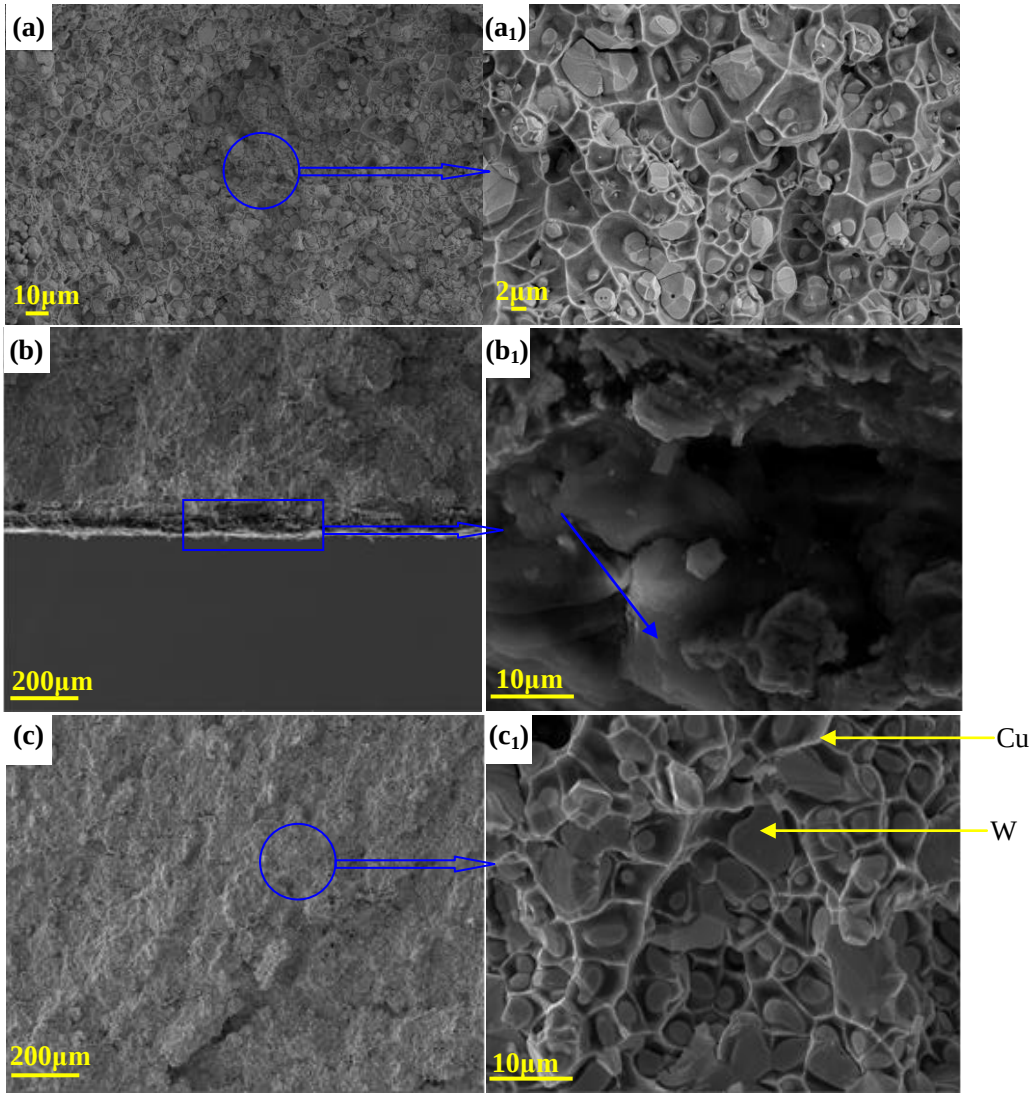

Fig. 7 Fracture morphology of the W-Cu composites before and after carburization at 1100°C with a dwell time of 30h: (a, a_1) Uncarburized W-Cu composites, (b, b_1) surface and (c, c_1) matrix of carburized W-Cu composites.

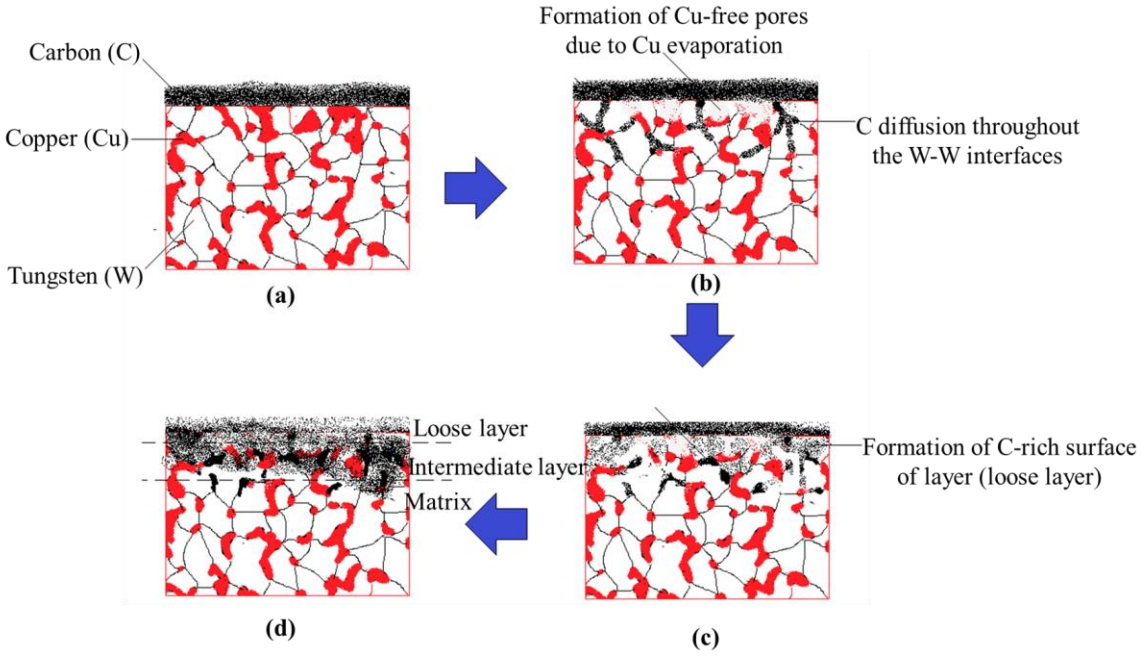

Fig. 8 The schematic diagram of W-Cu composite carburization process

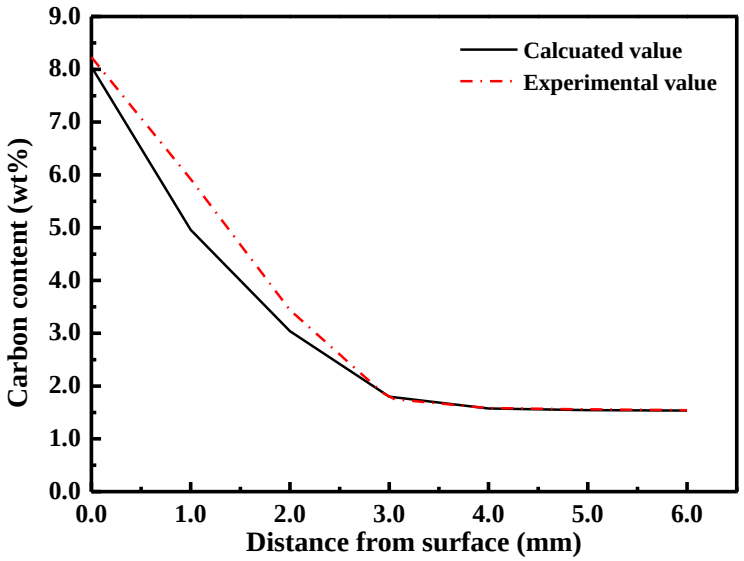

Fig. 9 Results of carbon concentration distribution of W-Cu composites after carburization at 1100^{o}C, obtained from analysis based on Fick's 2nd Law and experimental measurement.

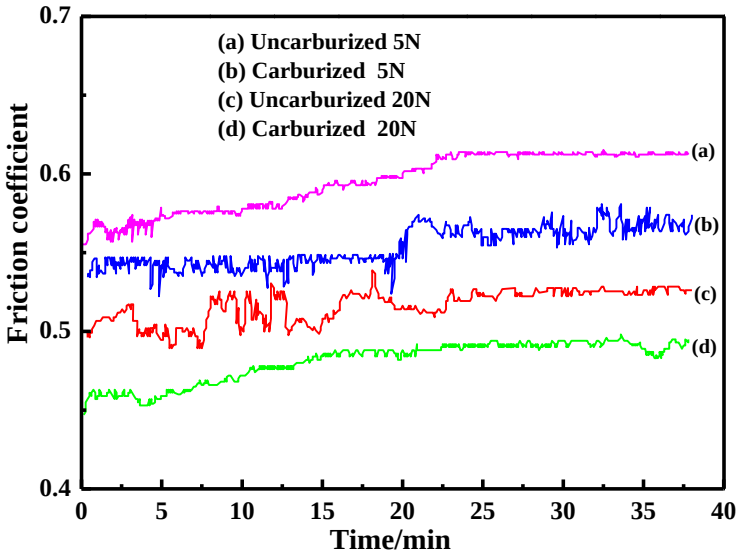

Fig. 10 Friction coefficient curve of W-Cu composite after carbonization at 1100^{o}C under different applied loads measured and sliding time.

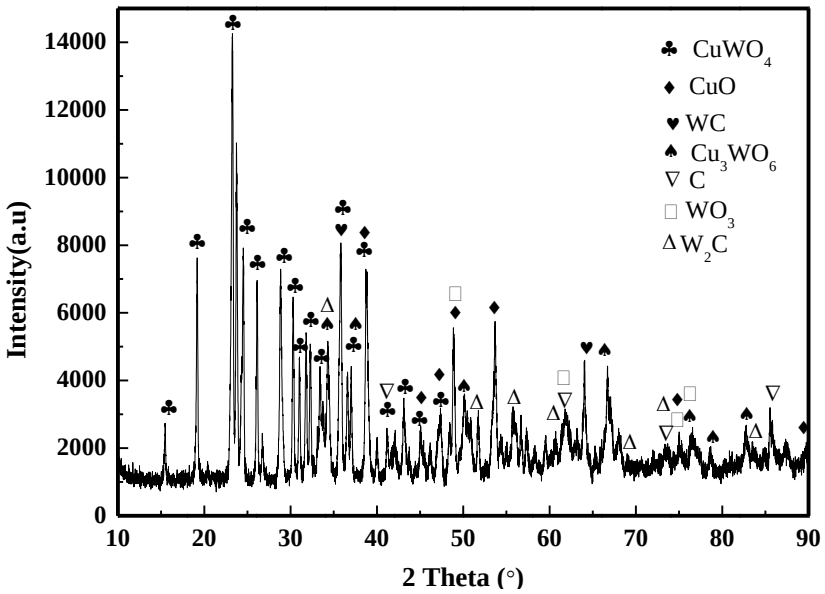

Fig. 11 The XRD pattern of W-Cu composites after high temperature wear.

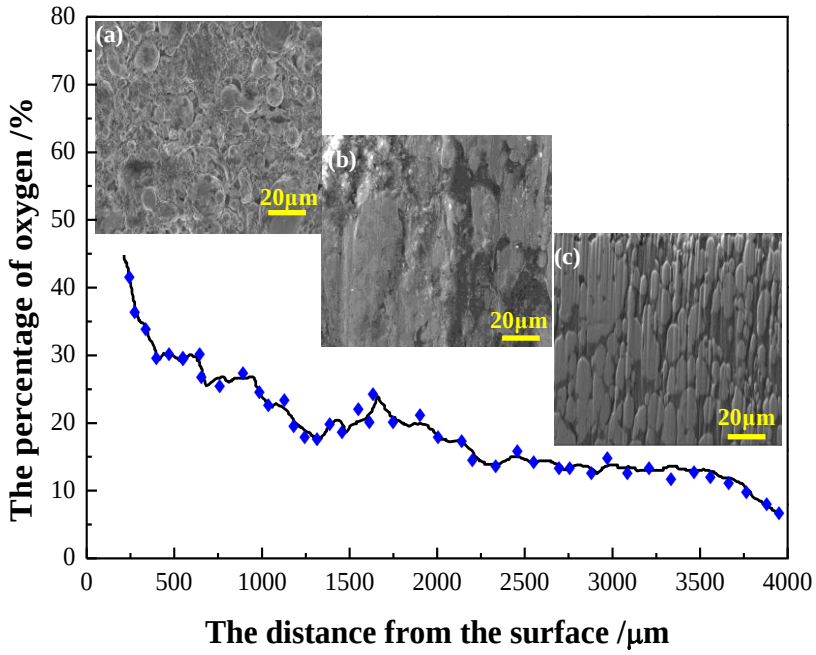

Fig. 12 The content of oxygen and SEM images of W-Cu composite wear at 900 ^{o}C.